



HAL
open science

Study on effect of pore structure on the permeability of concrete after a century natural carbonation

Yunyun Tong, Zhixiang Li, Mengya Li, Jiong Wang, Abdel-Okash Seibou, Jinjian Ye

► **To cite this version:**

Yunyun Tong, Zhixiang Li, Mengya Li, Jiong Wang, Abdel-Okash Seibou, et al.. Study on effect of pore structure on the permeability of concrete after a century natural carbonation. *Journal of Asian Architecture and Building Engineering*, 2022, 22 (5), pp.2867-2875. 10.1080/13467581.2022.2160642 . hal-04219833

HAL Id: hal-04219833

<https://hal.science/hal-04219833>

Submitted on 27 Sep 2023

HAL is a multi-disciplinary open access archive for the deposit and dissemination of scientific research documents, whether they are published or not. The documents may come from teaching and research institutions in France or abroad, or from public or private research centers.

L'archive ouverte pluridisciplinaire **HAL**, est destinée au dépôt et à la diffusion de documents scientifiques de niveau recherche, publiés ou non, émanant des établissements d'enseignement et de recherche français ou étrangers, des laboratoires publics ou privés.



Study on effect of pore structure on the permeability of concrete after a century natural carbonation

Yunyun Tong, Zhixiang Li, Mengya Li, Jiong Wang, Abdel-Okash Seibou & Jinjian Ye

To cite this article: Yunyun Tong, Zhixiang Li, Mengya Li, Jiong Wang, Abdel-Okash Seibou & Jinjian Ye (2023) Study on effect of pore structure on the permeability of concrete after a century natural carbonation, Journal of Asian Architecture and Building Engineering, 22:5, 2867-2875, DOI: [10.1080/13467581.2022.2160642](https://doi.org/10.1080/13467581.2022.2160642)

To link to this article: <https://doi.org/10.1080/13467581.2022.2160642>



© 2022 The Author(s). Published by Informa UK Limited, trading as Taylor & Francis Group on behalf of the Architectural Institute of Japan, Architectural Institute of Korea and Architectural Society of China.



Published online: 29 Dec 2022.



Submit your article to this journal [↗](#)



Article views: 414



View related articles [↗](#)



View Crossmark data [↗](#)

Study on effect of pore structure on the permeability of concrete after a century natural carbonation

Yunyun Tong^a, Zhixiang Li^a, Mengya Li^b, Jiong Wang^a, Abdel-Okash Seibou^b and Jinjian Ye^a

^aSchool of Civil Engineering and Architecture, Zhejiang University of Science & Technology, Hangzhou, China; ^bLaboratory of Mechanics and Materials of Civil Engineering (L2MGC), CY Cergy Paris Université, Cergy, France

ABSTRACT

The durability of concrete is determined by its pore structure and permeability. The present work examines the effect of pore structure and porosity on the permeability of concrete after nearly a century natural carbonation. The samples were cored from a concrete building built in 1931. X-ray diffraction analysis, phenolphthalein dye test, Mercury Intrusion Porosimetry (MIP) were conducted to ascertain the composition, the carbonation depth, the permeability, the porosity and pore size distribution of samples. The experimental results revealed that the front of core samples was completely carbonated. The fractal dimension was calculated using the Mandelbrot model to characterize the pore structure. The combined harmless and less harmless pore proportions exhibited a linear correlation with the fractal dimension. A relationship between permeability and fractal dimension is established. The increase in the fractal dimension resulted in a gradual decrease in the oxygen diffusion coefficient. The diffusion coefficient tends to plateau when the fractal dimension exceeds a critical value of the combined pore proportion. While the pore proportion of concrete was higher than 14.64%, there was no significant effect on the permeability. The results of this study can serve for future assessments of concrete durability.

ARTICLE HISTORY

Received 15 September 2022
Accepted 16 December 2022

KEYWORDS

Natural carbonation;
concrete; permeability;
fractal dimension; pore
structure

1. Introduction

Permeability is one of the main factors determining the durability of concrete. This parameter can be defined as the degree of penetration, diffusion or migration of gases, liquids or ions under the action of pressure, chemical potential or electric field (Fidjestøl and Lewis 2019). Concrete materials are porous and heterogeneous. Its permeability is primarily dependent on the pore size and size distribution, both of which can affect the extent of intrusion by harmful media. For example, the permeability of concrete can affect the degree to which carbon dioxide enters the material. This is important because carbon dioxide is capable of corroding steel reinforcement bars. The diffusivity of oxygen through concrete will also occur in response to a concentration gradient and will promote the rusting of steel reinforcement structures. Thus, permeability has a significant effect in terms of determining the durability of concrete structures.

As noted, the permeability of concrete is primarily a function of porosity (Li et al. 2019). Pore structures additionally affect the physical and mechanical properties of concrete, such as strength, energy at break, toughness, elasticity, effective diffusivity and durability (Beaudoin, Feldman, and Tumidajski 1994). The pore structures in concrete can be analyzed based on the fractal theory, using fractal dimensions to characterize

various indicators of structural complexity on specific size scales (Lü et al. 2019). According to (Mandelbrot 1984), fractals are self-similar structural patterns that appear on specific scales and can be characterized by a fractal dimension. Various complex structures, such as the Menger sponge and Apollonian spheres (Borkovec, De Paris, and Peikert 1944), are fractals and can be generated by simple iterations of specific patterns. These fractal structures can affect certain natural processes, such as liquid diffusion (Zeng 2018), osmosis and crystal nucleation (Zeng 2017; Zeng and Xu 2015; Yan et al. 2016).

Numerous studies have applied the fractal theory to comprehend the heterogeneity and complexity of concrete and interpret its durability. A prediction model of permeability has been developed by Wang, Guo, and Wang (2022), while the fractal dimension was used to evaluate the roughness of textile-reinforced concrete and a good correlation has been reported. Jin et al. (Jin, Zheng, and Yu 2020) evaluated the fractal dimension of concrete before and after freeze-thaw and used it as the independent variable for a mathematical damage model to analyze its durability. The results confirmed that the fractal dimension can be used to predict the damage degree of concrete. Fan and Zhang found that there is a decreasing linear relationship between fractal dimension of pore structure and freeze-thaw

CONTACT Mengya Li  mengya.li1@cyu.fr  Laboratory of Mechanics and Materials of Civil Engineering (L2MGC), CY Cergy Paris Université, 5 mail Gay Lussac, 95000 Cergy, Neuville-sur-Oise, France

© 2022 The Author(s). Published by Informa UK Limited, trading as Taylor & Francis Group on behalf of the Architectural Institute of Japan, Architectural Institute of Korea and Architectural Society of China.

This is an Open Access article distributed under the terms of the Creative Commons Attribution License (<http://creativecommons.org/licenses/by/4.0/>), which permits unrestricted use, distribution, and reproduction in any medium, provided the original work is properly cited.

attack, while the fractal dimension can also be used to evaluate the damage to adhesive interface (Fan and Zhang, 2021). Research on concrete pavements has indicated that the fractal method and fractal dimension can describe quantitatively the water permeability and address the durability challenges (Xie, Akin, and Shi 2019).

The porosity and pore distribution of concrete are strongly affected by carbonatation. The transformation of portlandite into calcium carbonate induces an increase in the volume of the solid phase, a reduction of porosity and an alteration of pore structure (Ngala and Page 1997). However, few studies have been devoted to the relationship between the modified pore structure after carbonation and permeability. The aim of this work was to investigate the correlations between pore structure, porosity and permeability of the carbonated concrete. The samples were cored from a historical building of early 20th century in China. The permeability and pore structure of concrete were determined experimentally, and fractal dimension was calculated to characterize the pore structure. The mathematical models were established between microscopic parameters and macroscopic performance in order to provide reference data for the further exploitation of durability.

2. Sampling and methods

2.1. Sampling preparation

The Zhejiang Library is a two-story building that incorporates classical roman orders, built in 1931, located

on 102 Da'xue Road in the Shang Cheng District, Hangzhou, Zhejiang Province, China (Figure 1). The reinforced concrete structure has an area of around 3000 m². In August 1997, the building was designated as a protected site and also a provincial cultural relic. In October 2019, the site was listed on China's national cultural relics protection unit. At present, the overall layout, architectural form and style of the facility are basically well preserved, though the basement, floor, concrete beams, columns and roof have degraded to varying degrees.

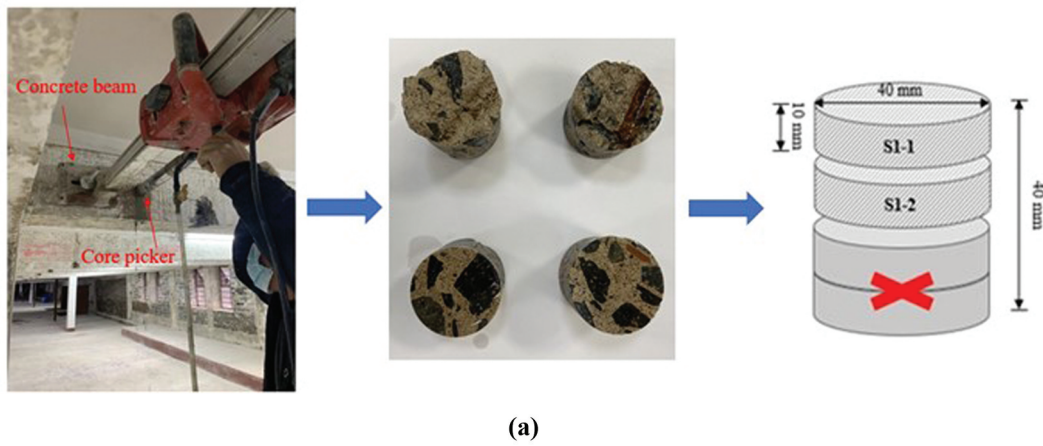
The concrete investigated in this work was acquired from concrete beams in the basement of this site. In order to avoid hitting the rebar during drilling, the positions of the reinforcement rebar were marked by a Profometer PM-6 rebar detector. The core picker of HZ-18 was used to extract the samples from concrete beam. The samples were cylinder-shaped, with a diameter of 40 mm and a depth of 40 mm. The samples were then sliced to two pieces of 10 mm (Figure 2(a)). S1, S2, S3, S4 and S5 were used to represent the specimens cored from the different locations as shown in Figure 2(b). The physical parameters of concrete samples are recapitulated in Table 1.

2.2. X-ray diffraction

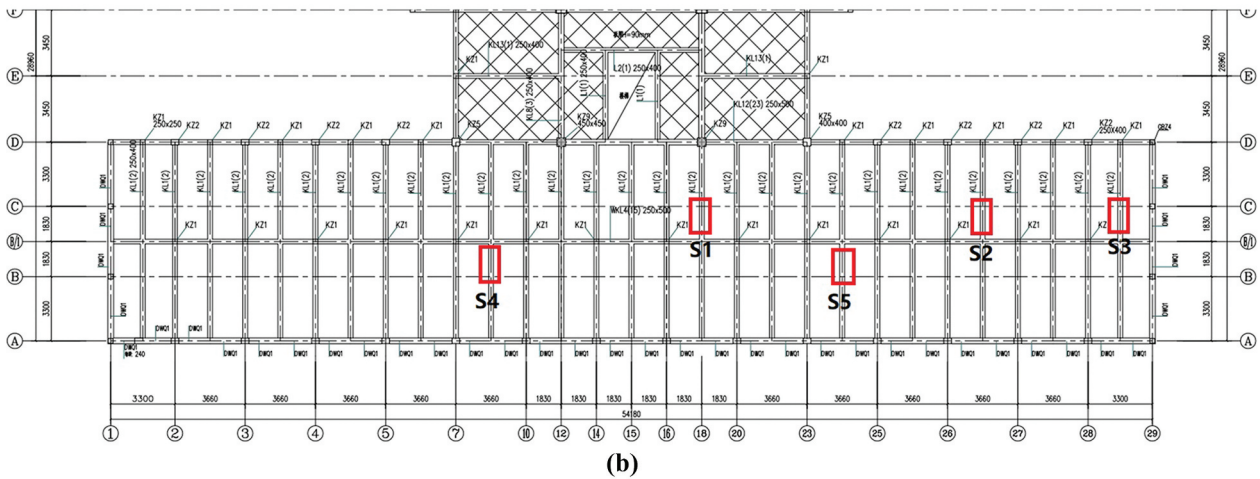
The three ingredients of concrete can be clearly seen from the cross section of the sample (Figure 3(a)), including cement, sand and coarse aggregate, respectively. The samples were then separated into coarse aggregate and mortar. The



Figure 1. Zhejiang library in Hangzhou, China.



(a)



(b)

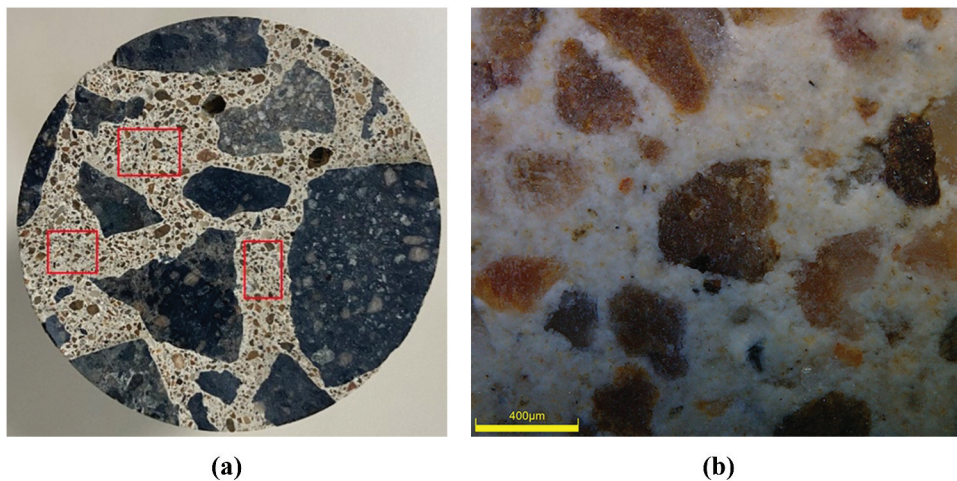
Figure 2. Illustration of sampling preparation (a) coring process (b) sampling locations.

Table 1. Physical characteristics of concrete samples.

Parameter	Value
Concrete density (kg/m ³)	2160
Finesse modulus of fine aggregate	2.3–3.0
Coarse aggregate density (kg/m ³)	2220
Particle size of coarse aggregate (mm)	14–30

current study focused on the pore structure of mortar, and the micro morphology observed by

microscope is presented in Figure 3(b). Each paste was crushed to obtain fragments each with a mass of approximately 10 g, and these crushed cement pastes were subsequently heated at 60°C in an oven (XMTA-600) for 48 h. Then, the specimens were allowed to cool for 6 h in the room. Following this, each cement mortar was crushed in a shredder and then passed through a 320-mesh sieve. The powdered materials that passed



(a)

(b)

Figure 3. Cross section of sampling (a) macro morphology of concrete sample surface and (b) micro morphology of mortar.



Figure 4. Specimens used for carbonation depth analysis.

through the sieve were analyzed by X-ray diffraction (XRD) using an Ultima VI Model X diffractometer.

2.3. Carbonation depth analysis

The surface of concrete samples were sprayed with a 1% phenolphthalein indicator solution according to EN 14630 (EN 14630:2007). The depth of the sampling was 40 cm, and the carbonation had reached up to 38.5 cm deep as indicated in Figure 4. The building is located in the province with high average annual relative humidity, while carbonation is boosted.

2.4. Oxygen diffusion measurement

The permeability values of the various specimens were determined using an oxygen diffusion apparatus. The samples were heated at 60°C in an oven for 3 d, then removed, weighed, and placed back in the oven. Following this, the samples were weighed again at 6 h intervals until the mass change between two consecutive weighing was not more than 0.01 g. The dried samples were then transferred into polyethylene (vinyl chloride) tubes that were sealed with epoxy resin.

Once the epoxy resin has completely hardened, concrete specimens were placed in the experimental apparatus for measuring the oxygen diffusivity (Zhou et al. 2018). Vaseline was applied to the chamber's mouth to ensure an airtight seal, as shown in Figure 5. The oxygen diffusivity measurement was based on Fick's first law, from which the oxygen concentration gradient can be used to determine the permeation factor.

The device was divided into left- and right-side gas chambers and high-purity oxygen passed into the left chamber, while high-purity nitrogen flowed into the right chamber. Different oxygen concentrations were obtained in the two chambers by closing the left and right valves as well as the ventilation valves. The oxygen diffusion coefficient D_f can be calculated (Zhou, Jin, and Fu 2018; Sercombe et al. 2007) as:

$$D_f = \frac{N}{\left(\int_0^t \left[\frac{dC}{dx}\right] dt\right) \cdot S} \quad (1)$$

and,

$$\frac{dC}{dx} = \frac{C_2 - C_1}{d} = \frac{\Delta C}{d} \quad (2)$$

where N is the total amount of oxygen that has diffused at a given point in time during the test, S is the

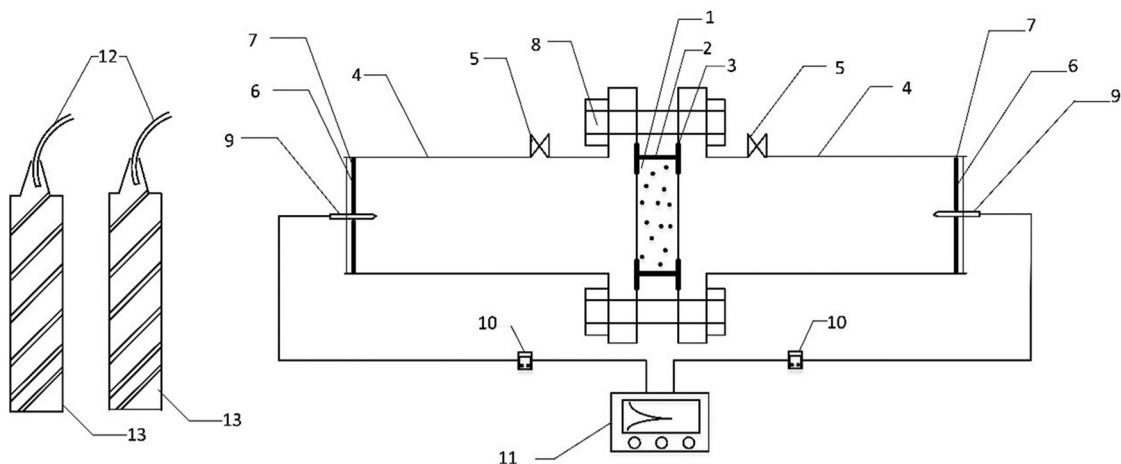


Figure 5. Experimental apparatus of oxygen diffusion measurement (Zhou, Jin, and Fu 2018). Legend: 1 = Concrete specimen; 2 = Epoxy resin; 3 = Rubber sealing gasket; 4 = Chamber tube wall; 5 = Intake valve; 6 = Move the piston; 7 = Piston seals; 8 = Stud bolts; 9 = Oxygen sensor; 10 = Oxygen concentration tester; 11 = Data logger; 12 = Gas catheter; 13 = Gas cylinders.

effective diffusion area, C_2 is the concentration of oxygen in the hyperoxide chamber at a specific point in time, C_1 is the oxygen concentration in the other chamber at the same time, d is the specimen thickness, and t is the total time span over which the oxygen diffused.

2.5. Pore structure measurement

The Mercury Intrusion Porosimetry (MIP) technique was used to assess the pore structures of the specimens, employing the PM 20 apparatus. A maximum pressure of 420 MPa was applied during these analyses, with a contact angle of 140° and the pore size measurement range was 0.0036 to 10.66 μm. Samples were prepared by crushing the concrete specimens to produce fragments 2–3 mm in size. These materials were oven dried at 60°C for 48 h and then allowed to cool naturally prior to being assessed.

2.6. Fractal model

The complexity of the pore structure in a material is reflected by its fractal dimensions as originally defined by (Mandelbrot 1984). Many researchers (Han, Wang, and Feng 2022; Gao et al. 2022) have studied the correlation between fractal dimensions and the porosity of concrete materials, as well as connections with the strength and elastic modulus of concrete, as a means of connecting macroscopic properties with microscopic characteristics. In the present work, a fractal model based on thermodynamics was used to calculate the fractal dimensions of the concrete beam pore structures. The model used for these calculations assumed cylindrical pores was proposed by Zhang and Li (1995), which was the same assumption applied for the mercury pressure experiments. This model was improved by Chen et al. (2004) such that it can be employed to directly calculate the fractal dimensions of pore structures based on mercury pressure data, using the mercury injection pressure, injection volume and pore size as inputs. The improved thermodynamic fractal model can be written as:

$$\ln\left(\frac{W_n}{r_n^2}\right) = D_s \ln Q_n + \ln C \tag{3}$$

where n is the number of intervals at which pressure is applied during this process, r_n is the pore size corresponding to the n^{th} mercury inlet (m), C is a constant and D_s is the fractal dimension of the pore surfaces. W and Q represent accumulated intrusion work in the

first n steps and cumulative invasive mercury volume in the first n steps, are expressed as follows:

$$W_n = \sum_{i=1}^n \bar{P}_i \Delta V_i \tag{4}$$

and

$$Q_n = \frac{\sqrt[3]{V_n}}{r_n} \tag{5}$$

where \bar{P}_i is the average pressure for the i^{th} mercury inlet operation (Pa), ΔV_i is the amount of mercury uptake for the same operation (m^3). V_n is the cumulative amount of mercury uptake over the pressure intervals from 1 to n (m^3).

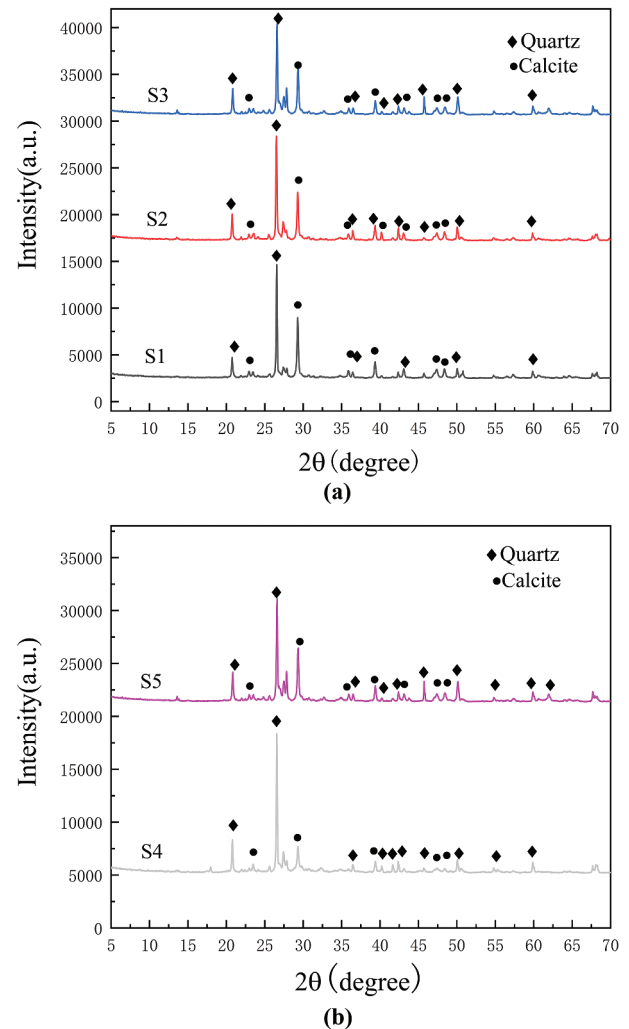


Figure 6. XRD patterns of five specimens (a) S1-S3 (b) S4-S5.

Table 2. Cement mortar compositions determined by XRD.

	S1	S2	S3	S4	S5
SiO ₂	66.5	65.4	61.4	59.2	66
CaCO ₃	33.5	34.6	38.6	40.8	34

3. Results and discussion

3.1. Mineralogy

The XRD diffraction patterns of five specimens are presented in Figure 6. The profiles were fitted by Rietveld's full-spectrum via Jade[®]. The compositions of specimens are summarized in Table 2.

The XRD results show that the cement mortar in the concrete beams in this area of the building comprised only silicon dioxide and calcium carbonate. Compounds such as calcium hydroxide were not found, which indicated that the first slice (10 mm) of samples have been completely carbonated. The results obtained were in accordance with phenolphthalein dye test. The binder used was Portland cement, and the ratio of sand to cement was approximately 6.4:3.6 which was given the average of five samples.

3.2. Gas permeability

The equations concerning the oxygen concentration gradient to time based on Eq. (2) were used to calculate permeability, and the fitting functions are summarized in Table 3.

The logistic regressions to the oxygen concentration gradient versus time data gave the best fits and

the resulting oxygen diffusion coefficients are presented in Table 4. It can be noted that S2 exhibited higher oxygen diffusion coefficient than other samples. A probable reason is that S2 was less durable, while the pore structure of the sample has been subjected to more alterations. Another likely explanation is that the sample contained the ink-bottle shaped pores (Lü et al. 2019). When mercury penetrates the narrow bottleneck of this shaped pore, a higher intrusion pressure will be injected to fill the pores, leading to a higher diffusion value.

3.3. Pore structure

Concrete is a heterogeneous material containing both harmless and less harmless cut-off pores, which tend to promote frost resistance and reduce the permeability of the material. Wu and Lian proposed a pore classification system based on their size range (Wu and Lian 1999). Harmless pores were defined as those between 0 and 20 nm in size, whereas less harmless pores were defined as those between 20 and 50 nm. The pore size distributions of the present samples were calculated, and the results are shown in Table 5. It can be observed that the pore characteristics of specimen S2-1 were not as evident as others, which is due to the injection of

Table 3. Oxygen concentration gradient versus time fitting functions.

S1-1	Linear	$y = -1.09175x + 9657.52384$	$R^2 = 0.99500$
	Exponential	$y = 9348.14055e^{-0.0555 \frac{x}{35881}} + 499.26507$	$R^2 = 0.99998$
	Logistic	$y = \frac{16480.35331}{1 + \left(\frac{x}{11373.83993}\right)^{1.00075}} - 6628.05999$	$R^2 = 0.99999$
S1-2	Linear	$y = -0.45777x + 7440.39533$	$R^2 = 0.99797$
	Exponential	$y = 5676.68774e^{-\frac{x}{10472.90629}} + 1812.57357$	$R^2 = 0.99992$
	Logistic	$y = \frac{14149.63346}{1 + \left(\frac{x}{29155.32664}\right)^{0.96347}} - 6650.8377$	$R^2 = 0.99994$

Table 4. Oxygen diffusion coefficients.

Specimen	Oxygen diffusion ($\times 10^{-8}$ m ² /s)
S1-1	3.71
S1-2	4.11
S2-1	7.99
S2-2	13.28
S3-1	4.00
S3-2	8.35
S4-1	3.86
S4-2	8.35
S5-1	6.19
S5-2	4.36

Table 5. Porosity values and pore size distributions of samples.

Specimen	Porosity [%]	Aperture distribution ratio [%]		
		0–20 nm	20–50 nm	Harmless and less harmless
S1-1	16.70	5.03	9.61	14.64
S1-2	18.58	5.54	12.58	18.12
S2-1	18.62	0	3.39	3.39
S2-2	19.30	3.72	8.07	11.79
S3-1	24.25	7.65	13.31	20.96
S3-2	22.26	2.13	7.13	9.26
S4-1	19.85	10.26	5.45	15.71
S4-2	21.08	4.63	4.89	9.52
S5-1	19.57	1.14	6.73	7.87
S5-2	17.98	8.18	18.80	26.98

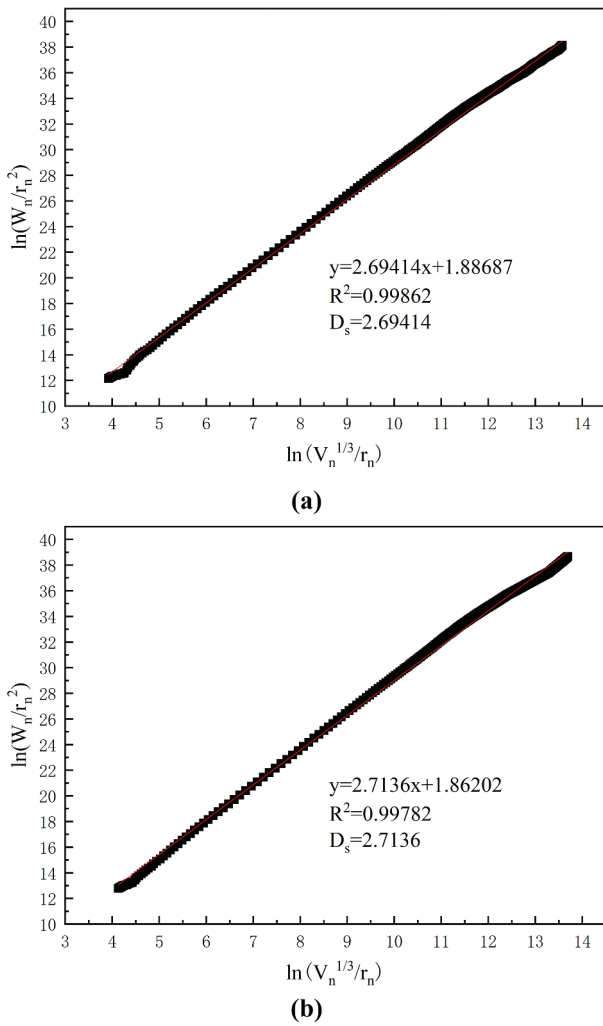


Figure 7. Plots used to determine the fractal dimensions of pore structures for two representative specimens (a) S1-1 (b) S1-2.

higher intrusion pressure; the inner volume measured can be smaller than the actual (Kim, Choi, and Choi 2018).

The proportion of harmless pores was relatively low in most samples, whereas the combined proportions of harmless and less harmless pores were in the range of 3.39% to 26.98%. These levels of porosity would be expected to affect the durability of the material. It is well known that the concrete oxygen diffusion can be increased by higher porosity. Nevertheless, no direct

Table 6. Fractal dimensions of the pore structures.

Specimen	D_s	R^2
S1-1	2.6941	0.9986
S1-2	2.7136	0.9978
S2-1	2.5851	0.9968
S2-2	2.6600	0.9981
S3-1	2.6837	0.9990
S3-2	2.6565	0.9971
S4-1	2.7165	0.9991
S4-2	2.6438	0.9969
S5-1	2.6632	0.9968
S5-2	2.7970	0.9989

correlation was found in our work between porosity and the oxygen diffusion coefficient.

3.4. Fractal dimension

The fractal dimensions of the concrete pore structures within the carbonated regions were determined using Equations (3), (4) and (5) according to the mercury pressure data. The experimental results of porosimetry were used to draw the bi-logarithmic plot with $\ln(\sqrt[3]{V_n}/r_n)$ and $\ln(W_n/r_n^2)$ by Excel. Representative linear fitting results, including the correlation between R^2 and the slope of the linear, are presented in Figure 7 and the numerical results are recapitulated in Table 6. In the concept of three-dimensional Euclidean space, the fractal dimension D_s of a porous structure should be a real positive number, which is less than 3. The same conclusion has been conducted by (Neimark 1990). As indicated in Table 6, the fractal dimensions of the pore structures were in the range of 2.5851 to 2.7970 with R^2 values for the plots all greater than 0.99. These high correlations confirm the validity of calculating fractal dimensions based on the thermodynamic model.

3.5. Parameter correlations

The correlation between the fractal dimension and the oxygen diffusion coefficient is plotted in Figure 8, which shows fractal dimension values in the range of 2.5851 to 2.6941. The results confirm that an increase in the fractal dimension gradually decreases the oxygen diffusion coefficient. Li et al. reported the same relationship between fractal dimension and permeability of heterogeneous rock (Li 2010). One reason why the permeability has decreased is that increasing the fractal dimension leads to a more complex pore structure, which makes it more difficult for oxygen to spread throughout the concrete. However, the diffusion

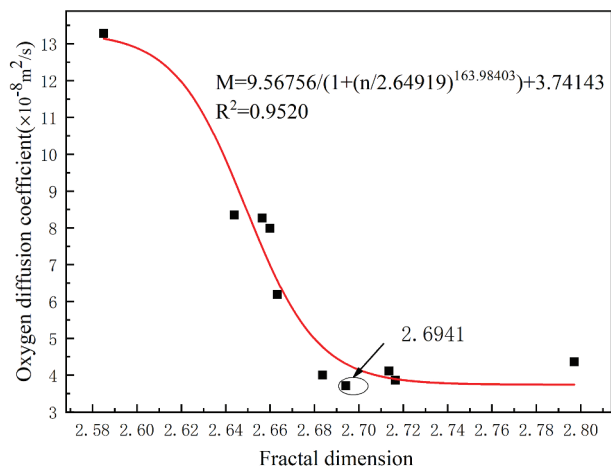


Figure 8. Relationship between fractal dimension and oxygen diffusion coefficient.

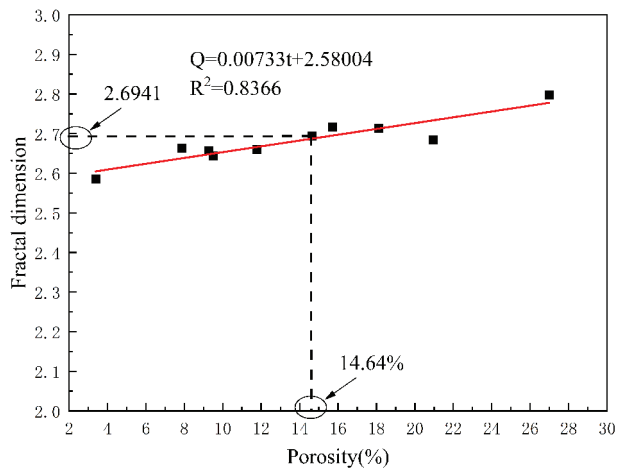


Figure 9. Relationship between the fractal dimension for the pore structure and the combined proportion of harmless and less harmless pores.

coefficient plateaued at a fractal dimension of approximately 2.6941, maintaining a value of approximately $4 \times 10^{-8} \text{ m}^2/\text{s}$. Consequently, under certain conditions, the oxygen diffusion coefficient can be reduced and the impermeability of concrete can be improved by reducing the fractal dimension of the pore structure.

It would be helpful to establish relationships between the fractal dimensions and the harmless and less harmless pore proportions in concrete as a means of assessing durability. The present work found that the fractal dimensions were closely correlated with the pore size proportions, as shown in Figure 9. The fractal dimension evidently increased with increases in the combined proportion of harmless and less harmless pores. This finding is in accordance with prior work by Wang et al. (Wang, Dong, and Li 2021), who reported a good linear correlation between the fractal dimension of steel-polypropylene fiber concrete and the harmless and less harmless pore proportion. The correlation proved that the porosity has a bearing on the fractal dimension. Therefore, under certain conditions, the pore size distribution of concrete can be assessed based on the fractal dimension of the pore structure. In addition, the magnitude of the fractal dimension can be increased by increasing the combined proportion of harmless and less harmless pores, which in turn reduces the oxygen diffusion coefficient and improves the durability of the material. According to the linear fitting curves generated in the present study, a combined pore proportion of 14.64% was associated with a fractal dimension of 2.6941. The linear correlation shows that the proportion of harmless and less harmless pores obviously influences the complexity of pore

structure. The same results have been reported by Gao, Wu, and Yuan (2021).

4. Conclusion

The conclusions of this study can be summarized as follows:

- (1) The concrete samples investigated in this study have been completely carbonated after about a century natural carbonation.
- (2) The pore size distribution was determined by MIP, and Mandelbrot model was used to calculate fractal dimension.
- (3) The fractal dimension can effectively characterize the pore structure and pore size distribution. A linear correlation was established between the fractal dimension and porosity. An increase in pore proportion can give rise to the fractal dimension.
- (4) A mathematical model was proposed to describe the relationship between fractal dimension and oxygen diffusion coefficient. It was found that the permeability decreased with the increase in fractal dimension up to a critical value. No further reduction of permeability can be observed when the pore (width smaller than 50 nm) proportion is higher than 14.64%.

Highlights

- The nature carbonated concrete specimens are cored from a historical building built in early 20th.
- The pore structure of carbonated concrete is analyzed by Mercury Intrusion Porosimetry (MIP) and characterized by fractal theory.
- The relationship between fractal dimension and permeability of the natural carbonated concrete is investigated.
- The fractal dimension shows a significant correlation with gas permeability.

Disclosure statement

No potential conflict of interest was reported by the author(s).

Funding

This work was supported by the Key Projects of the National Natural Science Foundation of Zhejiang Province [LY19E080002]; Zhejiang Science and Technology Project of Cultural Relics Preservation [2019014].

References

- Beaudoin, J. J., R. F. Feldman, and P. J. Tumidajski. 1994. "Pore Structure of Hardened Cement Paste and Its Influences on Properties." *Advanced Cement Based Materials* 1 (5): 224–236. doi:10.1016/1065-7355(94)90028-0.
- Borkovec, M., W. De Paris, and W. R. Peikert. 1944. "The Fractal Dimension of the Apollonian Sphere Packing." *Fractals* 2 (4): 521–526. doi:10.1142/S0218348X94000739.
- Chen, S. Q., Y. Z. Liu, G. X. Cheng, and C. B. Huang. 2004. "Computation on Surface Fractal Dimension of freeze-dried Product by Mercury Porosimetry." *Food Science* 25 (7): 25–29. EN 14630. 2007. "Determination of Carbonation Depth in Hardened Concrete by the Phenolphthalein Method. British Standard." *European standard*.
- Fan J. C., and B. Zhang. 2021. "Repair of Ordinary Portland cement Concrete Using Alkali Activated slag/fly Ash: Freeze-thaw Resistance and Pore Size Evolution of Adhesive Interface." *Construction and Building Materials* 300: 124334. doi:10.1016/j.conbuildmat.2021.124334.
- Fidjestøl, P., and R. Lewis. 2019. "Microsilica as an Addition." *Lea's Chemistry of Cement and Concrete* 5: 509–535.
- Gao, S., Y. Ji, Z. W. Qin, H. W. Zhang, F. Xing, and A. Liu. 2022. "A Comprehensive Analysis of Pore Structures and Performances of Mineral Admixtures Modified Recycled Aggregate Concrete Based on Experiment and Theory." *Construction and Building Materials* 358: 19451. doi:10.1016/j.conbuildmat.2022.129451.
- Gao Y., K. Wu, and Q. Yuan. 2021. "Limited Fractal Behavior in Cement Paste upon Mercury Intrusion Porosimetry Test: Analysis and Models." *Construction and Building Materials* 276: 122231. doi:10.1016/j.conbuildmat.2020.122231.
- Han, X., B. M. Wang, and J. J. Feng. 2022. "Relationship between Fractal Feature and Compressive Strength of Concrete Based on MIP." *Construction and Building Materials* 322: 12504. doi:10.1016/j.conbuildmat.2022.126504.
- Jin S. S., G. P. Zheng, and J. Yu. 2020. "A Micro freeze-thaw Damage Model of Concrete with Fractal Dimension." *Construction and Building Materials* 257: 119434. doi:10.1016/j.conbuildmat.2020.119434.
- Kim J. Y., Y. C. Choi, and S. Choi. 2018. "Fractal Characteristics of Pore Structures in GGBFS-based Cement Pastes." *Applied Surface Science* 428: 304–314. doi:10.1016/j.apsusc.2017.09.165.
- Li, K. 2010. "Analytical Derivation of Brooks–Corey Type Capillary Pressure Models Using Fractal Geometry and Evaluation of Rock Heterogeneity." *Journal of Petroleum Science and Engineering* 73 (1–2): 20–26. doi:10.1016/j.petrol.2010.05.002.
- Li, L. G., J. J. Feng, J. Zhu, and S. H. Chu. 2019. "Pervious Concrete: Effects of Porosity on Permeability and strength." *Magazine of Concrete Research* 73 (2): 1–35.
- Lü, Q., Q. L. Qiu, J. Zheng, J. Y. Wang, and Q. Zeng. 2019. "Fractal Dimension of Concrete Incorporating Silica Fume and Its Correlations to Pore Structure, Strength and Permeability." *Construction and Building Materials* 228: 11986. doi:10.1016/j.conbuildmat.2019.116986.
- Mandelbrot, B. B. 1984. "The Fractal Geometry of Nature." *Journal of the Royal Statistical Society* 147 (4): 616–618. doi:10.2307/2981858.
- Neimark, A. V. 1990. "Calculating Surface Fractal Dimensions of Adsorbents." *Adsorption Science & Technology* 7 (4): 210–219. doi:10.1177/026361749000700402.
- Ngala V. T., and C. L. Page. 1997. "Effects of Carbonation on Pore Structure and Diffusional Properties of Hydrated Cement Pastes." *Cement and Concrete Research* 27 (7): 995–1007. doi:10.1016/S0008-8846(97)00102-6.
- Sercombe, J., R. Vidal, C. Gallé, and F. Adenot. 2007. "Experimental Study of Gas Diffusion in Cement Paste." *Cement and Concrete Research* 37 (4): 579–588. doi:10.1016/j.cemconres.2006.12.003.
- Wang, C. X., J. M. Dong, and D. S. Li. 2021. "Research on Frost Resistance of Hybrid Fiber Reinforced Concrete Based on Fractal Theory of Pore Structure." *Bulletin of the Chinese Ceramic Society* 40 (11): 3608–3616.
- Wang, B. X., J. H. Guo, and J. Q. Wang. 2022. "Prediction Method of Permeability of textile-reinforced Concrete Based on Fractal Dimension Theory." *Construction and Building Materials* 327: 126868. doi:10.1016/j.conbuildmat.2022.126868.
- Wu, Z. W., and H. Z. Lian. (1999). *High Performance Concrete*. Beijing: China Railway Publishing House. in Chinese.
- Xie N., M. Akin, and X. M. Shi. 2019. "Permeable Concrete Pavements: A Review of Environmental Benefits and Durability." *Journal of Cleaner Production* 210: 1605–1621. doi:10.1016/j.jclepro.2018.11.134.
- Yan, D., Q. Zeng, S. Xu, Q. Zhang, and J. Wang. 2016. "Heterogeneous Nucleation on Concave Rough Surfaces: Thermodynamic Analysis and Implications for Nucleation Design." *The Journal of Physical Chemistry* 120: 10368–10380.
- Zeng, Q. 2017. "A Simple Method for Estimating the Size of Nuclei on Fractal Surfaces." *Journal of Crystal Growth* 475: 49–54. doi:10.1016/j.jcrysgro.2017.05.037.
- Zeng, Q. 2018. "Size Matching Effect on Wenzel Wetting on Fractal Surfaces." *Result Physics* 10: 588–593. doi:10.1016/j.rinp.2018.07.010.
- Zeng, Q., and S. Xu. 2015. "Thermodynamics and Characteristics of Heterogeneous Nucleation on Fractal Surfaces." *The Journal of Physical Chemistry* 119: 27426–27433.
- Zhang, B. Q., and S. F. Li. 1995. "Determination of the Surface Fractal Dimension for Porous Media by Mercury Porosimetry." *Industrial & Engineering Chemistry Research* 34 (4): 1383–1386. doi:10.1021/ie00043a044.
- Zhou, L. Q., N. G. Jin, and C. Q. Fu. 2018. "Determination Method and Testing Device of Oxygen Diffusion Coefficient of cement-based Material." *Experimental Technology and Management* 35 (7): 117–120.
- Zhou, L. Q., N. G. Jin, C. Q. Fu, Y. Tian, and H. Y. Jiang. 2018. "Prediction Model of Oxygen Diffusion in Cement-based Materials under Dry Condition." *Journal of the Chinese Ceramic Society* 46 (8): 1133–1140.